Correlation between static and dynamic polarimetric properties and the texture of surface-stabilised ferroelectric liquid crystal cells

Matthieu Dubreuil, P. Babilotte, Sylvain Rivet, Bernard Le Jeune, Laurent Dupont

HAL Id: hal-00822974

https://hal.univ-brest.fr/hal-00822974v1

Submitted on 15 May 2013

Liquid crystals

Correlation between static and dynamic polarimetric properties and the texture of Surface-Stabilized ferroelectric liquid crystal cells

Matthieu Dubreuil[1,2,*], Philippe Babilotte[1,2], Vinicius N. H. Silva[3], Sylvain Rivet[1,2], Bernard Le Jeune[1,2] and Laurent Dupont[3]

[1]*Université Européenne de Bretagne, 5 boulevard Laennec 35000 Rennes, France*

[2]*Université de Brest, Laboratoire de Spectrométrie et Optique Laser (EA 938), 6 avenue Le Gorgeu, C.S. 93837, 29238 Brest Cedex 3, France*

[3]*Département d'Optique (UMR CNRS 6082), Telecom Bretagne, Technopôle Brest-Iroise, C.S. 83818, 29238 Brest Cedex 3, France*

*corresponding author. Email: matthieu.dubreuil@univ-brest.fr

Correlation between static and dynamic polarimetric properties and the texture of Surface-Stabilized Ferroelectric Liquid Crystal cells

Snapshot Mueller matrix polarimetry was performed for static and dynamic analyses of surface-stabilized ferroelectric liquid crystal cells under electric field. A strong correlation between the static (at fixed voltage) and dynamic (upon field reversal) polarimetric properties and the texture of ferroelectric liquid crystal cells was established. The birefringence properties were different between a rooftop/zigzag-textured cell and a stripe-textured cell. The trajectory of the optical axis, plotted over the transition between two addressed states, was analyzed for each cell. The shape of the trajectories could be explained by a reversible motion of the smectic layers while switching.

1. Introduction

The description of static and dynamic effects in ferroelectric liquid crystal (FLC) cells in the surface-stabilized geometry has been widely investigated since their first implementation by Clark and Lagerwall [1]. A simple way to gain insight into the texture of such cells is to examine them with a polarizing microscope [2]. Furthermore, electro-optical characterization can be made by intensity measurements between crossed polarizers with a temporal resolution in the order of microsecond. However, the use of a complex model is required to get a complete description of the molecular distribution and the layer structure. But, other methods were developed to characterize liquid crystals (LCs), which are model-independent. Among them, X-ray diffraction, for example, allows the description of the layer structure [3]. Otherwise, optical guided modes [4] give access to the molecular in depth-distribution. However, with these last two methods, lateral spatial resolution as well as temporal resolution is often poor.

A snapshot Mueller matrix polarimeter [5] was recently developed by our team, and further used to carry out time-resolved analyses of reorientations in FLC cells [6]. This tool has many advantages for optical characterization of liquid crystals. First, the lateral spatial resolution is about the optical beam size (~500 µm here). Secondly, the temporal resolution, equal to the detector acquisition time (~µs here), is the best one

achievable among current Mueller polarimeters. Moreover, the Mueller matrix gives access independently to each polarimetric property of the sample (dichroism, birefringence and depolarization), which is more interesting than simple intensity measurements.

When a high-intensity and low-frequency electric field is applied to a Surface-Stabilized Ferroelectric Liquid Crystal (SSFLC) cell, its texture is known to evolve from an initial uniform texture with zigzag defects to a uniform striped texture by passing through a most complicated "rooftop" texture [7-10]. The change of texture is associated to the irreversible straightening out of the smectic layers, due to the coupling of the spontaneous polarization with the applied electric field. The electro-optical behavior of a cell was shown to be dependent on its texture [7].

The study reported here was aimed at establishing a strong correlation between the static and dynamic polarimetric properties (issued from Mueller matrix measurements) and the texture of SSFLC cells. We will show for dynamic measurements that, over the transition between two addressed states, the trajectory of the optical axis of the cell depends on its texture.

The experimental setup is described in Section 2. Then, the polarimetric parameters issued from Mueller matrix measurements are explained and related to the director distributions within the cell in Section 3. Section 4 gives insight into the textures of the SSFLC cells, and Section 5 presents the static (at fixed voltage) and the dynamic (upon field reversal) polarimetric parameters. Section 6 reports on the results of similar experiments carried out on a single cell made of areas of different textures, in order to check for the previous findings. Finally, the dynamic behavior of the liquid crystal molecules and the one of the smectic layers are discussed.

2. Experimental setup

The Snapshot Mueller Matrix Polarimeter (SMMP) used in this study was described in [5]: parallel polarization states are obtained by encoding through use of the spectral domain. Indeed, the aim is to assign a given state of polarization to a given wavelength. The device consists of a broadband source, a polarizer and two retarders for polarization state generation, plus two retarders, one polarizer and a dispersive system for polarization state analysis. The full polarimetric response (Mueller matrix) of the sample is thus included in a single spectrum, $I(\lambda)$, whose acquisition time only depends

on the detection system. The experimental setup is depicted in Figure 1.

[insert Figure 1]

The 15-nm-broad source is a superluminescent diode (B&WTek®) with a central wavelength at 829 nm. The beam size, initially around 1 mm, has been reduced to 500 µm by using an afocal system composed of two lenses. The polarizers (ColorPol®), made of nanoparticules, have an extinction ratio of 100 000:1 and an angular acceptance of 20°. The retarders are made of calcite ($\Delta n = 0.1661$), and have a thickness e = 2.08 mm for the coding system, whereas the thickness of those used for the decoding system is 5e = 10.4 mm. The light is collected by a multimode optical fiber, and injected into a dispersive system composed of a 1200 grooves/mm grating and a 512x512 pixels CCD camera (ICCD-Max®). Given that only one dimension of the CCD is used (wavelength axis), a binning is made in the other direction (intensity axis), which enhances the signal-to-noise ratio. In order to avoid coherence effects, the sample is imaged on a scattering medium, in turn imaged at the entrance of the optical fiber. The temporal characteristics of the camera for data acquisition are: a gate width adjustable over a time range from the ns to the s and a repetition rate around 1 kHz. A full Mueller matrix is included in a single spectrum, $I(\lambda)$, and thus recorded under the previous conditions, which are the best ones achievable among current Mueller polarimeters. The Mueller matrix is evaluated at the wavelength λ_0, which is the central wavelength of the detection range. Techniques for reconstruction of Mueller matrices and calibration of the device were described in [11].

3. Polarimetric parameters

All of the polarimetric properties of a given sample are contained in its Mueller matrix. They consist of: i) dichroism (action on the electric field component amplitudes), ii) birefringence (action on the electric field component phases) and iii) depolarization (random action on both amplitude and phase). For liquid crystal analysis under normal incidence, no dichroism is expected. On the other hand, such devices have a strong birefringence effect. A liquid crystal cell can thus be associated to a retarder. The depolarization effect results from a spatial (over the section of the beam seen by the detector) or/and temporal (over the acquisition time) averaging of polarimetric properties. However, spatial inhomogeneities create scattering of light. In the setup described here (Figure 1), spatial filtering is achieved by the pinhole, which means that

there is no collection of the scattered/diffracted light. If spatial inhomogeneities create scattering, no depolarization will be detected. However, depolarization will be used, through the depolarization index, P_D [12], to control the aperture time of the CCD camera.

The different polarimetric effects are separated by a Lu and Chipman decomposition of each experimental Mueller matrix [13]. It results in the analysis of three matrices (diattenuation, retardance and depolarization matrices), corresponding to each polarimetric effect (dichroism, birefringence, depolarization). In this study, only the retardance matrix was exploited. The advantage of measuring the whole Mueller matrix of the sample and performing a Lu and Chipman decomposition is that the birefringence properties are obtained from the resolution of an over-determined and noise-filtered system. A set of 3 experimental parameters giving the full description of the retarder associated to the liquid crystal cell can be extracted from the retardance matrix: they consist of i) the retardance (R, phase difference between the two eigenstates of the retarder), ii) the azimuth angle (α_R, direction of the fast axis of the retarder) and iii) the ellipticity angle (ε_R, ellipticity of the retarder). Those parameters are totally model-independent, and they only describe the way the polarization of the light is modified by the cell. The first two parameters (α_R and R) can be used to represent the optical axis of the retarder into the laboratory coordinate system (O_X, O_Y, O_Z), as shown in Figure 2.

[Insert Figure 2]

Indeed, a liquid crystal cell can always be described by a homogeneous uniaxial slab, where the direction of the optical axis is totally determined by the knowledge of 2 angles, the in-plane angle, θ_{in}, and the off-plane angle, θ_{off}. In the measurements presented here, those 2 angles are linked to R and α_R as follows:

$$\alpha_R = \theta_{in} \tag{1}$$

$$R = \frac{2\pi\Delta n\left(\theta_{off}\right)d}{\lambda_0} \qquad \text{with} \qquad \Delta n\left(\theta_{off}\right) = \frac{n_e n_o}{\sqrt{n_e^2 \sin^2\left(\theta_{off}\right) + n_o^2 \cos^2\left(\theta_{off}\right)}} - n_o \tag{2}$$

with $\lambda_0 = 829$ nm, d is the thickness of the SSFLC cell, n_e and n_o are, respectively, the extraordinary index and the ordinary index of the liquid crystal cell. The parameter, α_R, which is equal to θ_{in}, is thus the angle between the projection of the optical axis in the

plane of the glass plates and the rubbing direction. The parameter, R, is linked to the angle, θ_{off}, which is the angle between the optical axis and the glass plate. Under the assumption of a uniform in-depth molecular distribution, the optical axis is aligned with the long axis of the molecules (director).

The last parameter (ε_R) is linked to the in-depth molecular distributions (along O_Z). It was shown [14] that, along the direction of the light propagation, a superposition of linear retarder slabs with their optical axis in different directions is equivalent to an elliptic retarder. This is the case for "twist" or "splayed" molecular distributions along the depth. Although the ellipticity parameter ε_R is not sufficient to get an in-depth-resolved description of the molecular orientation (one should generate a distribution and compare the result of light propagation with the experimental parameters), it can give insight into the global shape of the distribution. For example, simple distributions were simulated to quantify the ellipticity parameter, for a 1.5 µm planar-oriented cell with a cone angle $\theta=25.5°$. For a uniform distribution, the ellipticity is 0°. For a quasi-uniform but symmetric chevron distribution as in [15], the ellipticity is also 0°, which can be explained by the perfect compensation of the twist between the two halves of the cell. For a splayed distribution (with a linear variation of the azimutal angle ϕ between the two surfaces), the ellipticity parameter is about 8.7°. For a half-splayed distribution, the ellipticity parameter is about 6.7°.

One should keep in mind that the optical parameters under study results from an averaging over the optical beam size. However, thanks to spatial filtering, the scattered/diffracted light is not analyzed. In the case of SSFLC cells, layering defects create scattering and a horizontal chevron structure (stripes) creates diffraction. The optical parameters are thus not sensitive to these last two effects.

4. Textures of FLC cells

The samples under study were two SSFLC cells made of the same material (Felix 015/100 from Clariant®), whose characteristics are given in Table 1.

[insert Table 1]

They were prepared as follows: two glass substrates were coated first with transparent electrodes of indium-tin-oxide (ITO) and then spin-coated with a layer of polyimide prior to rubbing in order to generate a planar orientation of the liquid crystal. The gap between the substrates was controlled by glass-bead spacers to get thicknesses of about

1.8 µm (cell 1) and 1.5 µm (cell 2). Then, the LC Felix 015/100 in isotropic phase was introduced into the cell by capillarity and cooled down to the SmC* phase, at room temperature. A high-intensity and low-frequency electric field treatment (10Hz - ±20V square wave voltage during 2 hours) was applied to each cell in order to change its texture. Because of their different thicknesses, it resulted in the formation of two different textured cells. Indeed, the electric field seen by the liquid crystal molecules was lower in cell 1 than in cell 2. Figure 3 shows polarizing microphotographs of two regions of both cells after electric field treatment, under a 10V voltage.

[insert Figure 3]

Cell 1 presents a lot of "rooftop" defects (Figure 3-(a)) as well as a small area with zigzag lines (Figure 3-(c)). On the other hand, cell 2 exhibits a more uniform texture with stripes (Figure 3-(b) and 3-(d)). When no voltage was applied to the cells, both were brought to extinction when placed between crossed-polarizers (uniform memory states).

Such textures can be explained as follows: initially, after cooling down from the smectic A* phase, the smectic layers adopt the well-known vertical chevron structure. When an electric field is applied perpendicular to the glass plates, the spontaneous polarization tends to align with the electric field, but in the vertical chevron structure, they are not totally aligned. If the field value is sufficiently high, the smectic layers begin to straighten out for alignment of the spontaneous polarization with the electric field and form, at first, the "rooftop" texture. This texture suggests a local variation of the chevron angle. Increasing the electric field (or the exposure time) makes the smectic layers evolve to the so-called quasi-bookshelf structure leading to the formation of a horizontal chevron structure seen as stripes under polarizing microscope. This irreversible behavior has been widely supported by both optical [7-10] and X-ray diffraction [16-18] measurements.

5. Static and dynamic polarimetric properties

Our investigations were focused, at first, on the static (at fixed voltage) polarimetric properties of the liquid crystal cells. The driving scheme of the applied voltage is depicted in Figure 4.

[Insert Figure 4]

The detection system and the driving voltage were synchronized in order to measure the polarimetric properties at 4 specific voltage values: +15V, 0V (from +15V), -15V and 0V (from -15V). The addressed states were those obtained at +15V ("up") and -15V ("down"), whereas the memory states were obtained at 0V from +15V ("0up") and -15V ("0down"). Relaxation times of about 1ms were determined from intensity measurements. To gain a global insight into the spatial distribution of polarimetric parameters over the cell, a polarimetric image of the cell was constructed, by moving the sample on a 2-D translation mount, and by measuring its Mueller matrix for each probing position. The distance between two probing positions was 500 µm; moreover, the image was composed of 400 "pixels" (20 x 20), which means with a global field of view of (1 cm x 1 cm). One should note that the independent behavior of the four states is not as useful as the comparison between the addressed and the memory states. For the two cells under study, Figure 5 shows variations in the values of α_R and R parameters between the "up" and "0up" states. Given the lack of significant difference between both states for ε_R and P_D, which are kept close to 0° and 1, respectively, they were not shown in this paper.

[insert Figure 5]

For cell 1, the average values of the differences are $<R^{up}-R^{0up}> = -4.90°$ and $<\alpha_R{}^{up}-\alpha_R{}^{0up}> = 7.20°$. For cell 2, the average values are $<R^{up}-R^{0up}> = -1.68°$ and $<\alpha_R{}^{up}-\alpha_R{}^{0up}> = 4.15°$. According to Figure 5, the memory states for cell 2 are closer to the addressed states than those of cell 1; this means that the difference is reduced by the electric field treatment. This result was confirmed by intensity measurements in a previous study [7]; in the investigations reported here, it is established for α_R and R.

The switching dynamics from the "up" to the "down" states ("up/down" transition) were then measured under application of a 100 Hz - ±15 V square wave voltage. In the current configuration of the experimental setup, the repetition rate of the CCD camera was around 1 kHz, and the switching times for the SSFLC cells were around 100 µs. The dynamic evolution of the polarimetric properties cannot, thus, be acquired over a single period. This led us to synchronize the camera with the applied voltage to further reconstruct the whole transition by a step by step lengthening of the acquisition delay. This process supposes that the molecules behavior is repeatable, which was verified otherwise. The acquisition time for one point and the step of the delay were both set equal to 5 µs. Figure 6 illustrates the dynamic evolutions of the polarimetric parameters, α_R and R, at one particular position (one pixel) within the cells.

[Insert Figure 6]

The depolarization index P_D, that has not been represented here, stays close to 1, which means that the acquisition time was short enough to avoid temporal averaging. The dynamic behaviors of α_R and R are very different between the two cells. For instance, the duration of the transition is shorter for cell 1 than for cell 2, as it can be seen on $\alpha_R(t)$ curves. The observation of $R(t)$ curves also shows two distinct behaviors. An interesting way to represent α_R and R is to draw the trajectory of the extremity of the $\overrightarrow{OA}$ vector over the transition, in the (O_Y, O_Z) plane, which is parameterized by the angles θ_{in} and θ_{off}, as it can be seen in Figure 2. The trajectories of $\overrightarrow{OA}$ vector in the (O_Y, O_Z) plane, corresponding to the experiments illustrated in Figure 6, were plotted in Figure 7. One should note that they were calculated under the assumption of unchanging indexes n_e and n_o during the transition, which means a collective motion of the molecules.

[insert Figure 7]

From Figure 7 it appears that the trajectory for cell 1 is flat-shaped whereas the one for cell 2 is more circular. To gain a global insight into this behavior, the "up/down" dynamics were investigated over the whole cells. Two parameters, $|S|$ and τ, were used to give account of the dynamic behavior. The parameter $|S|$ (expressed in degree) represents the flatness of the trajectory. It is defined as $|S| = \sum_i \left(\theta_{off}^i - \theta_{off}^0 \right)$, where θ_{off}^0 is the off-plane angle in the addressed state before the transition and θ_{off}^i is the off-plane angle for the ith acquisition of the transition. The parameter τ (expressed in microsecond) is the rise time of the transition, obtained by an adjustment of the equation

$\tan \theta_{in}(t) = \tan \theta \tanh \left[t/\tau - \ln \left(\tan \frac{\phi_0}{2} \right) \right]$ [19]. Their values were calculated for each

position of the cells, and the results are presented in Figure 8 as images set at the same spatial positions as in Figure 5 (static properties).

[Insert Figure 8]

It is worth noting that the behavior observed at one position of the two cells (a more flattened trajectory and a quicker transition for cell 1, Figures 6 and 7) is alike at every position in the cells.

In conclusion, the comparison of two cells with different textures showed that the optical axis of a cell with the texture of cell 1 (no stripes) has a more flattened trajectory during the transition than a cell textured as cell 2 (stripes), and that the rise time is shorter for cell 1 than for cell 2. Moreover, static experiments showed that the memory states are closer to the addressed states in cell 2 than in cell 1.

6. Results on a third cell having different textures

In order to validate the correlations exposed just above, the same experiments were carried out on a third and 1.6-µm-thick SSFLC cell (cell 3) made of the same material, but with zones of different textures. Indeed, the change of texture induced by the electric field treatment is very dependent on the original texture [20]. The results of the static and dynamic experiments are presented in Figure 9.

[insert Figure 9]

One should note that, for the static experiments, only the image representing the difference $\alpha_R{}^{up}-\alpha_R{}^{0up}$ is depicted, whereas for the dynamic characterization, only the trajectories at three particular positions of the cell are shown. The values of parameters $|S|$ and τ were calculated at these positions. The results of the static and dynamic experiments are presented in Table 2.

[Insert Table 2]

They show that, when the difference between memory and addresses states is decreasing, the trajectory of the $\overrightarrow{OA}$ vector becomes more and more circular, and that the rise time is increasing. This behavior corresponds to the behaviors of cells 1 and 2. Moreover, the static and dynamic behaviors are correlated to the inner textures of the cell. Indeed, at position 1, the texture is uniformly striped, at position 2, one can observe only a few stripes and at position 3 none of them is present. The indirect observation of the stripe texture was represented on Figure 9 as He-Ne laser light diffraction patterns.

The correlations between the texture and the static and dynamic behaviors of polarimetric parameters established for cells 1 and 2 are alike in the case of a single cell with different textures. Two conclusions can be made: i) the correlations are validated by the observations on cell 3, and ii) the static and dynamic polarimetric properties can be different over a single cell, depending on its local structure (chevron or quasi-bookshelf).

7. Discussion

The observations of the static and dynamic behaviors of polarimetric properties lead to several comments. First of all, the shape of the optical axis trajectory has to be discussed. During the "up/down" transition, the liquid crystal molecules are moving on the smectic cone [20] (Goldstone mode). Indeed, it has been verified that, for the three cells in question, the switching time is dependent on the applied voltage. If we assume a perfect bookshelf structure for the smectic layers and a uniform molecular distribution, the trajectory of the $\overrightarrow{OA}$ vector into the (O_Y, O_Z) plane should be a perfect circle. If the layers are tilted in a symmetric chevron structure, this trajectory is distorted toward a slightly deformed circle, because of the projection of the smectic cone system onto the laboratory system. But, if the layers are fixed, it is very unlikely that the $\overrightarrow{OA}$ vector will follow a flat-shaped trajectory over the transition. It is thus very likely that the smectic layers reorient reversibly while the director is moving around the cone. This behavior has already been proposed by other teams and compared with optical intensity measurements [21-22]. However, according to the experiments reported in [15] and [23], no reversible smectic layer movement upon field reversal was observed. It was suggested in [15] that the smectic layers remains unchanged and that the in-depth distribution of the molecules is quasi-uniform. Such a behavior cannot result in the observation of a flat-shaped trajectory for the $\overrightarrow{OA}$ vector. In [23], the authors proposed the formation of half-splayed states during switching. However, such a distribution would generate a high ellipticity parameter ε_R (see Section 3), that was never observed in this study, whatever the experiment (Figure 10). Moreover, in a recent study [24], the reversible reorientation of the smectic layers was observed in high resolution time-resolved X-ray experiments: it is worth recalling that such experiments are totally model-independent and give direct access to the organization of the layers. The results obtained by using the snapshot polarimeter are, thus, in agreement with the observation reported in [24].

This behavior could be explained by the strong influence of surface orientations in the SSFLC geometry. The interaction length of surface torques is in general much greater than the cell thickness, so the planar orientation at the surface imposes a planar orientation of the molecules in the whole cell. In addition, the structure of the SmC* phase forces the director to rotate on the smectic cone. To satisfy both requirements during switching, the smectic layers may move while the molecules are switching

around the cone, and keep them in the planar orientation over the whole transition. However, the chevron angle at the surfaces must be fixed, which probably results in a complicated deformed layer structure during the switching motion, as shown experimentally in static measurements [17]. This behavior also agrees with a previous description by Hartmann [21]. When the smectic layers are irreversibly straightened out further to the application of the electric field treatment, they are fixed in the quasi-bookshelf structure. As a consequence, the layers remain unchanged and steady during the switching process, and the trajectory of the $\overrightarrow{OA}$ vector into the (O_Y, O_Z) plane becomes close to a perfect circle, as observed experimentally here.

Although the above interpretation assumes a uniform or quasi-uniform distribution of the molecules, the case of the non-uniform distribution cannot be excluded. In that case, the representation as a trajectory is no more valuable, because the indexes n_e and n_o are time-dependent. However, the non-uniform distribution must evolve so as to fit the parameters R, α_R and ε_R during the whole transition. Although several non-uniform distributions have been proposed in the literature and confirmed by optical measurements [15,25], we found no theoretical distribution able to adjust Mueller parameters for our experiments.

[insert Figure 10]

There is another point that must be raised from the observations of the dynamic behaviors. Indeed, we showed that the transition was shorter in the chevron-structured (cell 1) than in the quasi-bookshelf-structured (cell 2). This result was confirmed by cell 3 (Table 2). This observations could be linked to the results proposed in [26,27] obtained by numerical calculations, where a longer delay time was ascribed to bookshelf cells. However, the rise time, that must scale inversely with the applied field, should be higher for position 3 than for position 1, because the effective applied field is stronger in position 1 than in position 3, through the term cos δ, where δ is the vertical chevron angle. The behavior observed here is the contrary.

8. Conclusion

This study established correlations between the static and dynamic polarimetric properties and the texture of surface-stabilized ferroelectric liquid crystal cells. For a cell exhibiting a texture with "rooftop" and zigzags defects (chevron structure), the

difference between addressed and memory states was found to be high. Moreover, the trajectory of the optical axis during the "up/down" transition proved to be flat-shaped. On the contrary, in a cell with a striped texture (quasi-bookshelf structure), the difference between addressed and memory states was lower, and the trajectory during the "up/down" transition was more circular. Assuming a collective movement for the molecules, the shape of the trajectories can only be explained by a reversible motion of the smectic layers, simultaneously to the rotation of the molecules on the smectic cone. This result has to be confirmed by carrying out local measurements by using time-resolved optical guided mode and X-ray methods. However, the experiments reported here show that the snapshot Mueller matrix polarimeter is a beneficial tool, thanks to its simplicity and high temporal resolution, and can lead to a better knowledge of dynamic behaviors into liquid crystal devices.

References

[1] Clark N.A. and Lagerwall S.T., "Submicrosecond bistable electro-optic switching in liquid crystals", *Appl. Phys. Lett.* **1980**, *36* (11), 899-901.

[2] Derking I., "*Textures of liquid crystals*", Wiley-VCH Verlag, 2003.

[3] Rieker T.P., Clark N.A., Smith G.S., Parmar D.S., Sirota E.B. and Safinya C.R., "Chevron Local Layer Structure in Surface-Stabilized Ferroelectric Smectic-*C* Cells", *Phys. Rev. Lett.* **1987**, *59*, 2658-2661.

[4] Elston S.J., Sambles J.R. and Clark M.G., "Determination of the Director Alignment in a Ferroelectric Liquid Crystal Device by Observation of Optical Modes", *J. Mod. Opt.* **1989**, *36*, 1019-1025.

[5] Dubreuil M., Rivet S., Le Jeune B. and Cariou J., "Snapshot Mueller matrix polarimeter by wavelength polarization coding", *Opt. Express*, **2007**, *15* (21), 13660-13668.

[6] Dubreuil M., Rivet S., Le Jeune B. and Dupont L., "Time-resolved switching analysis of a ferroelectric liquid crystal by snapshot Mueller matrix polarimetry", *Opt. Lett.* **2010**, *35* (7), 1019-1021.

[7] Hartmann W.J.A.M. and Luyckx-Smolders A.M.M., "The bistability of the surface-stabilized ferroelectric liquid-crystal effect in electrically reoriented chevron structures", *J. Appl. Phys.* **1990**, *67* (3), 1253-1261.

[8] Shao R.F., Willis P.C. and Clark N.A., "The field induced stripe texture in surface stabilized ferroelectric liquid crystal cells, *Ferroelectrics*, **1991**, *121*, 127-136.

[9] Verhulst A.G.H. and Stommels F.J., "Smectic C* local layer structure within texture lines studied with a (sub)micrometer optical measuring spot", *Ferroelectrics*, **1991**, *121*, 79-90.

[10] Patel J.S., Lee S-D and Goodby J.W., "Electric field induced layer reorientation in ferroelectric liquid crystals", *Phys. Rev. A*, **1989**, *40* (5), 2854-2856.

[11] Dubreuil M., Rivet S., Le Jeune B. and Cariou J., "Systematic errors specific to a snapshot Mueller matrix polarimeter", *Appl. Opt.*, **2009**, *48* (6), 1135-1142.

[12] Gil J.J. and Bernabeu E., "Depolarization and polarization indices of an optical system", *J. Mod. Opt.*, **1986**, *33*, 185-189.

[13] Lu S.Y. and Chiman R.A., "Interpretation of Mueller matrices based on polar decomposition", *J. Opt. Soc. Am. A*, **1996**, *13* (5), 1106-1113.

[14] Scharf T., "*Polarized Light in Liquid Crystals and Polymers*", John Wiley & Sons, Inc., Hoboken, New Jersey, 2007.

[15] Maclennan J.E., Handschy M.A. and Clark N.A., "Director reorientation dynamics in chevron ferroelectric liquid crystal cells", *Liq. Cryst.*, **1990**, *7* (6), 787-796.

[16] Takahashi Y., Iida A., Takanishi Y., Ogasawara T., Nakata M., Ishikawa K. and Takezoe H., "Dynamic local-layer response of surface-stabilized ferroelectric liquid crystals to a high electric field by time-resolved x-ray microdiffraction", *Phys. Rev. E*, **2003**, *67*, 051706-1.

[17] Oh-e M., Isogai M., Kitamura T., "X-ray studies on layer structure and bistability in ferroelectric liquid crystals", *Liq. Cryst.*, **1992**, *11* (1), 101-109.

[18] Bryant G.K. and Gleeson H.F., "Evolution of irreversible layer deformations in FLC devices caused by high electric field treatment", *Ferroelectrics*, **1998**, *214* (1), 35-42.

[19] M.A. Handschy and N.A. Clark, "Structures and responses of ferroelectric liquid crystals in the surface-stabilized geometry", *Ferroelectrics*, **1984**, *59*, 69-116.

[20] Lagerwall S.T., "*Ferroelectric and antiferroelectric liquid crystals*", Wiley-VCH Verlag, 1999.

[21] Hartmann W.J.A.M., Vertogen G., Gerritsma C.J., Sprang H.A.V. and Verhulst A.G.H., "SSFLC field-induced director pattern modulation described in terms of smectic layer bending", *Ferroelectrics*, **1991**, *113*, 257-268.

[22] Giesselmann F. and Zugenmaier P., "Coupled director and layer reorientation in layer tilted ferroelectric smectic liquid crystal cells", *Mol. Cryst. Liq.Cryst.*, **1993**, *237* (1), 121-143.

[23] Willis P.C., Clark N.A. and Safinya C.R., "Molecular director and layer response of chevron surface stabilized ferroelectric liquid crystals to low electric field", *Liq. Cryst.*, **1992**, *11* (4), 581-592.

[24] Gleeson H.F., Bryant G.K. and Morse A.S., "Time-resolved X-Ray scattering studies of reversible layer flexing in a surface stabilised ferroelectric liquid crystal device", *Mol. Cryst. Liq. Cryst.*, **2001**, *362*, 203-215.

[25] Zhuang Z, Clark N.A, Maclennan J.E, "Visible polarized light transmission spectroscopy of the electro-optic switching behaviour of surface stabilized ferroelectric liquid crystal cells", *Liq. Cryst.*, **1991**, *10*(3), 409-417.

[26] Xue J-Z, Handschy M. A., Clark N. A., "Electrooptical switching properties of uniform layer tilted surface stabilized ferroelectric liquid crystal devices", *Liq. Cryst.*, **1987**, *2*(5), 707-716.

[27] Xue J-Z, Handschy M. A., Clark N. A., "Electrooptic response during switching of a ferroelectric liquid crystal cell with uniform director orientation", *Ferroelectrics*, **1987**, *73*(1), 305-314

Figure 1. Experimental setup of the snapshot Mueller matrix polarimeter in the (*e,e,5e,5e*) configuration. The input polarizer is set at 0° and the output polarizer at 90°. The optical axes of the retarders are respectively oriented at 45°, 0°, 0° and 45°. The retarders are made of calcite and are 2.08-mm-thick (coding system) and 10.4-mm-thick (decoding system), respectively. The lens, L_1, images the sample under study on the scattering medium, whereas the lens, L_2, images the scattering medium at the optical fiber entrance. The scattered/diffracted light is filtered by a pinhole set before the decoding system.
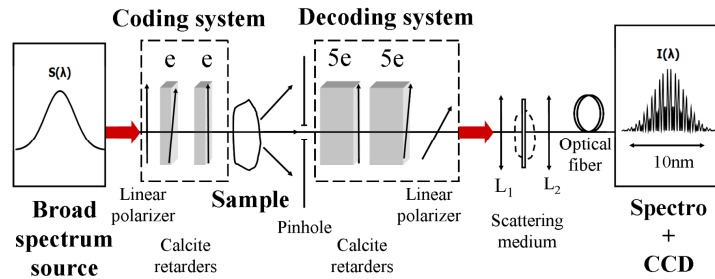
Figure 2. Representation of the cell in the laboratory coordinate system (O_X,O_Y,O_Z). The orientation of the optical axis is represented by $\overrightarrow{OA}$ vector.
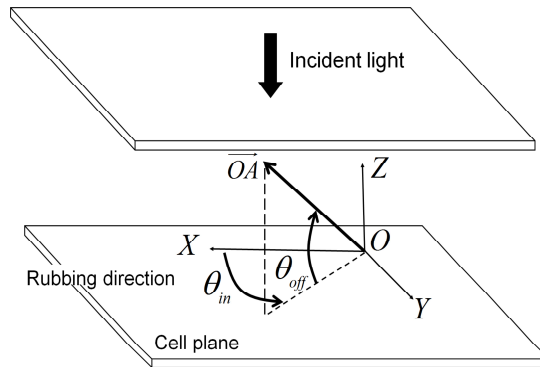
Figure 3. Textures observed under polarizing microscope for two areas of cell 1 ((a) and (c)) and cell 2 ((b) and (d)), after 2 hours of high-intensity and low-frequency electric field treatment (10Hz - ±20V). The polarizing microscope is the LEICA DMLP (10x objective). The field of view is (500 μm x 500 μm). The voltage applied to the cell is 10V, and the detection is synchronized with the driving voltage.
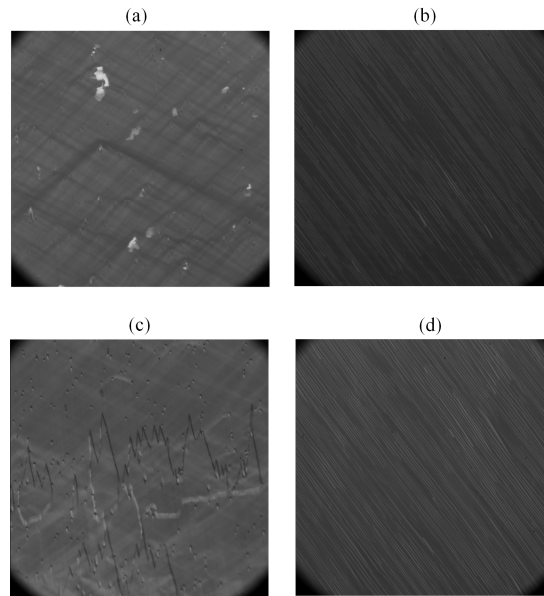
Figure 4. Trigger pulses (a) and driving scheme (b) of the applied voltage for the static experiments. The arrows indicate the position of the measurement for the "up", "0up", "down", "0down" states, are located respectively at *4ms*, *9ms*, *14ms* and *19ms* from the trigger pulse.
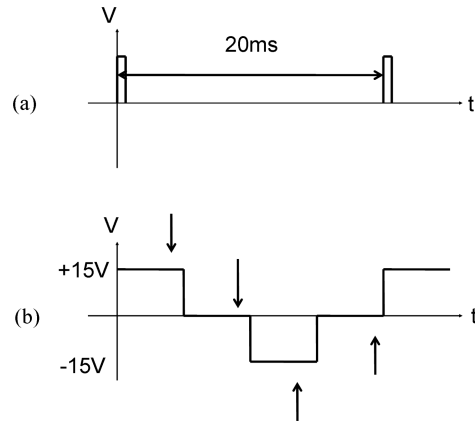
Figure 5. Comparison of the polarimetric parameter differences α_R and R between addressed ("up") and memory states ("0up"), for cell 1 and cell 2. The field of view is (1 cm x 1 cm). The vertical scale is in degree, and is divided into 50 gray levels.
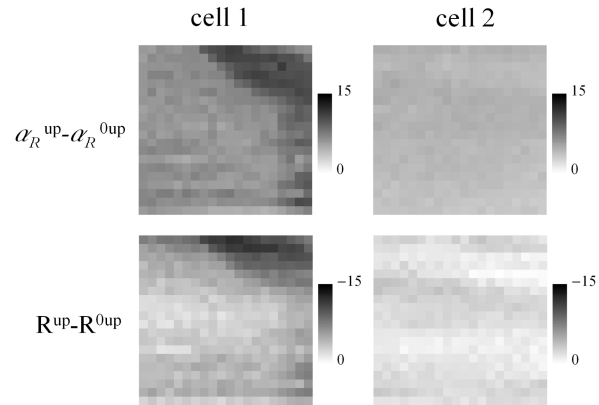
Figure 6. Dynamic evolution of the polarimetric parameters, α_R and R, during the "up/down" transition at one particular position of cell 1 and cell 2. The electric field is reversed at t = 50 μs; this time is represented by arrows on the figure.
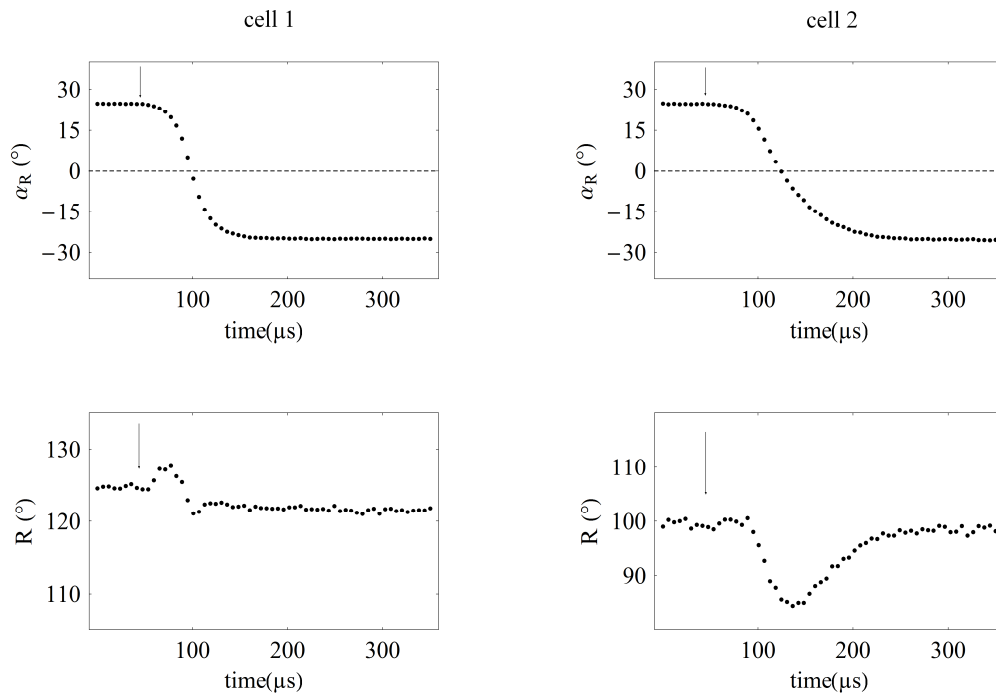
Figure 7. Trajectories of the extremity of the $\overrightarrow{OA}$ vector in the (O_Y, O_Z) plane corresponding to the experiments of Figure 6, for cell 1 and cell 2. The trajectory is parameterized by the angles θ_{in} and θ_{off}, defined in Figure 2.
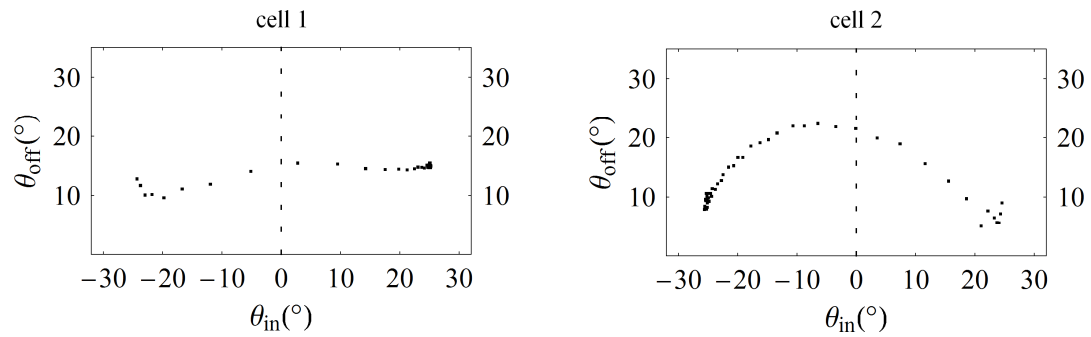
Figure 8. Images of parameters $|S|$ (°) and $\tau\,(\mu s)$, for cell 1 and cell 2. For explanations about the parameters see text. The spatial positions of the images are the same as the ones of Figure 5 (static properties). The average values for $|S|$ and τ are: for cell 1: $<|S|> = 52.9°$ and $<\tau> = 20.3\mu s$, and for cell 2: $<|S|> = 177.6°$ and $<\tau> = 36.5\mu s$.
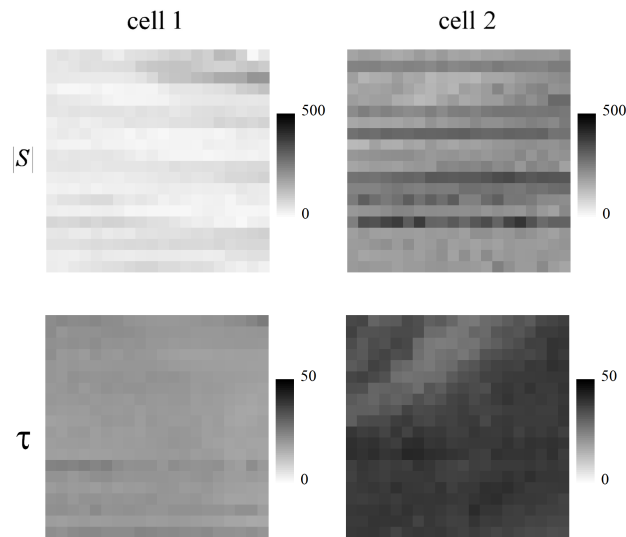
Figure 9. Static and dynamic experiments driven on cell 3. The static image represents the difference $\alpha_R{}^{up}-\alpha_R{}^{0up}$ in degree, with a (1 cm x 1 cm) field of view. The experimental trajectories of the optical axis are shown for three different probing positions. The photographs of He-Ne laser light diffraction patterns have been represented for each position.
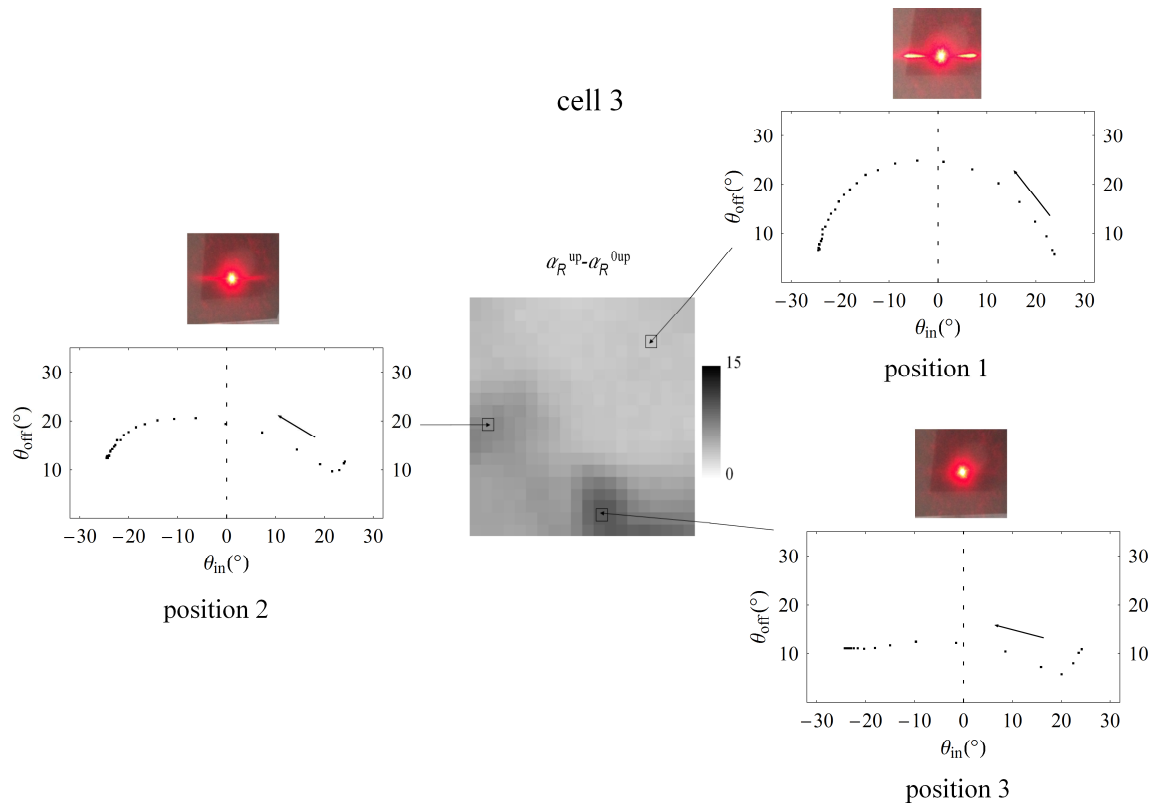
Figure 10. Evolution of the ellipticity parameter $\varepsilon_R(t)$ during the "up/down" transition at one position for cell 1 and cell 2.
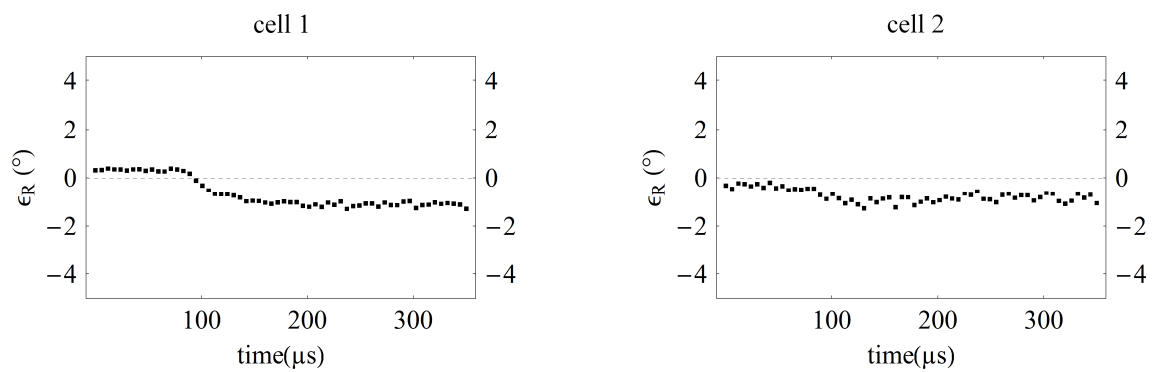
Table 1. Characteristics of the Felix 015/100 liquid crystal mixture.

spontaneous polarization P_S	$33 \ nC/cm^2$
viscosity η	$80 \ mPa.s$
tilt angle θ	$25.5°$
birefringence ($830nm$) Δn	0.16
phase temperature sequence	$X \xrightarrow{-12°C} C^* \xrightarrow{72°C} A^* \xrightarrow{83°C} N^* \xrightarrow{86°C} Isotropic$

Table 2. Values of the parameters $\alpha_R{}^{up}$-$\alpha_R{}^{0up}$, $|S|$, τ for the three positions within cell 3 (see Figure 9).

	position 1	position 2	position 3
$\alpha_R{}^{up}$-$\alpha_R{}^{0up}$ (°)	3	7	10
$|S|$ (°)	239.2	97.7	19.5
τ (µs)	29.5	23.5	16.9